Title

Conductivity of carbonate- and perfluoropolyether-based electrolytes in porous separators

Authors

Devaux, Didier
Chang, Yu H
Villaluenga, Irune
et al.

Publication Date

2016-08-01

DOI

10.1016/j.jpowsour.2016.05.039

Peer reviewed

Journal of Power Sources 323 (2016) 158–165

Contents lists available at ScienceDirect

Journal of Power Sources

journal homepage: www.elsevier.com/locate/jpowsour

Conductivity of carbonate- and perfluoropolyether-based electrolytes in porous separators

Didier Devaux [a, b, c], Yu H. Chang [a, c], Irune Villaluenga [a, b, c], X. Chelsea Chen [d], Mahati Chintapalli [d, e], Joseph M. DeSimone [f, g], Nitash P. Balsara [a, b, c, d, *]

[a] Environmental Energy Technologies Division, Lawrence Berkeley National Laboratory, Berkeley, CA 94720, USA
[b] Joint Center for Energy Storage Research (JCESR), Lawrence Berkeley National Laboratory, Berkeley, CA 94720, USA
[c] Department of Chemical and Biomolecular Engineering, University of California, Berkeley, CA 94720, USA
[d] Materials Science Division, Lawrence Berkeley National Laboratory, Berkeley, CA 94720, USA
[e] Department of Materials Science and Engineering, University of California, Berkeley, CA 94720, USA
[f] Department of Chemistry, University of North Carolina at Chapel Hill, Chapel Hill, NC 27599-3290, USA
[g] Department of Chemical and Biomolecular Engineering, North Carolina State University, Raleigh, NC 27695, USA

HIGHLIGHTS

- We report on the morphology and thermal properties of porous separators.
- Polyolefins and polytetrafluoroethylene separators were characterized.
- Carbonate- and perfluoropolyether-based electrolytes were investigated.
- Conductivity of electrolyte-separators composite is reported.
- Conductivity follows a master equation that depends on the electrolyte uptake only.

GRAPHICAL ABSTRACT

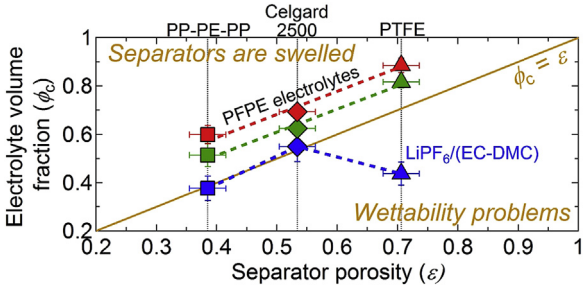

ARTICLE INFO

Article history:
Received 19 February 2016
Received in revised form
7 May 2016
Accepted 10 May 2016
Available online 20 May 2016

Keywords:
Perfluoropolyether
Conductivity
Separators
Battery
Polyolefin
Polytetrafluoroethylene

ABSTRACT

In lithium batteries, a porous separator filled with an electrolyte is placed in between the electrodes. Properties of the separator such as porosity and wettability strongly influence the conductivity of the electrolyte-separator composite. This study focuses on three commercial separators: a single layer polypropylene (Celgard 2500), a trilayer polypropylene-polyethylene-polypropylene (PP-PE-PP), and a porous polytetrafluoroethylene (PTFE). Electron microscopy was used to characterize the pore structure, and these experiments reveal large differences in pore morphology. The separators were soaked in both carbonate- and perfluoropolyether-based electrolytes. The conductivity of the neat electrolytes (σ_0) varied from 6.46×10^{-6} to 1.76×10^{-2} S cm^{-1}. The porosity and wettability of the separator affect the electrolyte uptake that in turn affect the conductivity of electrolyte-separator composites. The conductivity of the electrolyte-separator composites (σ) was found to follow a master equation, $\sigma = 0.51 \cdot \sigma_0 \cdot \varphi_c^{3.2\pm0.2}$, where φ_c is the volume fraction of the electrolyte in each separator.

1. Introduction

In lithium batteries, a porous separator filled with an electrolyte

* Corresponding author. Department of Chemical Engineering, 201 Gilman Hall, University of California, Berkeley, CA 94720-1462, USA.
E-mail address: nbalsara@berkeley.edu (N.P. Balsara).

http://dx.doi.org/10.1016/j.jpowsour.2016.05.039
0378-7753/

Table 1
Characteristics of separators. Thickness (l), porosity (ε), and onset melting and degradation temperatures (T_m, T_d).

Separator	l (μm)	ε	T_m (°C)	T_d (°C)
Celgard 2500	25.4 ± 0.6	0.53 ± 0.03	154	311
PP-PE-PP	25.5 ± 0.5	0.39 ± 0.03	129 & 156	347
PTFE	36.6 ± 0.8	0.71 ± 0.03	320	527

Table 2
Electrolyte uptake (EU) of electrolyte-separator composites.

	$LiPF_6$/(EC-DMC)	$PFPE_{E10H}$	$PFPE_{DMC}$
Celgard 2500	1.68 ± 0.14	3.04 ± 0.09	4.32 ± 0.12
PP-PE-PP	0.83 ± 0.06	1.94 ± 0.12	2.86 ± 0.15
PTFE	0.46 ± 0.03	3.49 ± 0.14	6.32 ± 0.08

is placed in between the electrodes [1,2]. The main functions of the separator are to act as a physical barrier to prevent short-circuit between the two electrodes and to allow ion transport. Microporous polyolefin membranes, made of semi-crystalline polymers such as polyethylene (PE) and polypropylene (PP), are widely used in commercial Li-ion battery [3,4]. These separators are designed to possess several physical and chemical properties that are important for the functioning of Li-ion batteries such as good mechanical properties, chemical and electrochemical stability, and compatibility with the chemical species involved in the redox reactions.

Ion transport within the electrolyte-separator composite depends on several factors such as the porosity and tortuosity, the electrolyte resistance, and the wettability of the pores by the electrolyte [5–8]. Notably, Saito et al. used measurements of the diffusion coefficients of the cation, anion and solvent species to conclude that interactions between the separator wall and electrolyte solution play a role on the ion transport efficiency [9]. The presence of the separator leads to a conductivity that is lower than that of the neat electrolyte. This increase in resistance affects battery performance [10–12]. In this paper, we study the conductivity of a series of electrolyte-separator composites.

The electrolytes of interest are low molecular weight perfluoropolyethers (PFPEs) doped with a lithium salt [13,14]. PFPEs are chemically resistant, non-crystalline, and nonflammable

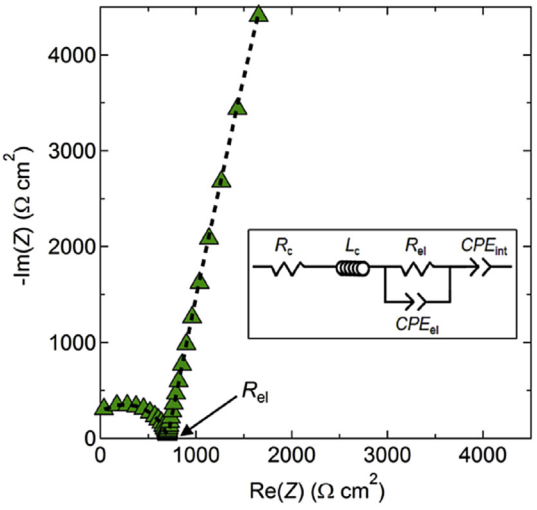

Fig. 1. AC impedance spectrum at 40 °C of the $PFPE_{E10H}$–Celgard 2500 composite. The symbols are the experimental data and the dashed line corresponds to the best fit using the electrical equivalent circuit shown in the inset.

fluorinated compounds that exhibit low glass transition temperature and low toxicity. We recently demonstrated that electrolytes with hydroxyl- and dimethyl-carbonate-terminated PFPEs can be used in Li batteries. They may provide a safe alternative to conventional alkyl-carbonate-based electrolytes. Currently there is no knowledge on the conductivity of PFPE-based electrolyte-separator composites. The present study includes two PFPE-based electrolytes and a conventional carbonate-based electrolyte. The three electrolytes are studied in three commercial separators: a single layer PP (Celgard 2500), a trilayer PP-PE-PP manufactured by the Celgard Company, and a porous polytetrafluoroethylene (PTFE) manufactured by the 3M Company, designed to serve as support for gas permeation membranes [15]. The conductivity of the neat electrolytes studied here differ by three orders of magnitude. The wettability of the electrolytes also differs widely; one expects the carbonate-based electrolyte to wet the polyolefin separators and the PFPE-based electrolytes to wet the PTPE separator. In spite of these differences, we show that the conductivity of all the electrolyte-separator composites follows a master equation. This equation quantifies the dependence of the conductivity of the electrolyte-separator composite on the neat electrolyte conductivity, the volume fraction of electrolyte in the separator, and a morphological factor that account for the tortuosity and the connectivity of the conducting phase within the separators.

2. Experimental

2.1. Electrolyte preparation

Ethoxylated alcohol-terminated perfluoropolyether (Fluorolink E10-H, Solvay Co.) ($PFPE_{E10H}$) with nominal molecular weight of 1.2 kg mol^{-1} was purchased from Alfa Aesar. Dimethyl carbonate-terminated perfluoropolyether ($PFPE_{DMC}$) was obtained by functionalization of hydroxyl-terminated PFPE (Fluorolink D10-H, Solvay Co.) ($PFPE_{D10H}$) with nominal molecular weight of 1 kg mol^{-1} using a method described previously [13]. Inside a MBraun glovebox maintaining an argon atmosphere with ultralow concentrations of water and oxygen, the two PFPEs were dried at room temperature in the glovebox antechamber for 3 days. Lithium bis(trifluoromethanesulfonyl)imide (LiTFSI, Novolyte Co.) was also dried in the same manner. Afterward, the PFPEs and LiTFSI were mixed at room temperature for three days. The weight percent of LiTFSI added in $PFPE_{E10H}$ and $PFPE_{DMC}$ was 9.1% and 9.6%, respectively. For control experiments, a conventional liquid electrolyte, 1 M $LiPF_6$ in a mixture of ethylene carbonate (EC) and dimethyl carbonate (DMC) in a 1:1 vol ratio ($LiPF_6$/(EC-DMC)) was purchased from Sigma Aldrich and used as received. Based on the product datasheet, the density (ρ_{el}) at room temperature of the $PFPE_{E10H}$, $PFPE_{D10H}$, and $LiPF_6$/(EC-DMC) are 1.73, 1.81, and 1.3 g cm^3, respectively. For the conductivity model developed in this paper, the density of the $PFPE_{DMC}$ is assumed to be identical to that of $PFPE_{D10H}$. The density of the PFPE-based electrolytes is considered similar to that of the neat polymer.

2.2. Commercial separators

A single layer polypropylene (PP) separator (Celgard 2500) was kindly provided by the Celgard Company. From the material datasheet, the reported thickness and porosity of the Celgard 2500 separator were 25 μm and 0.55, respectively. A trilayer polypropylene-polyethylene-polypropylene (PP-PE-PP) separator, also manufactured by the Celgard Company, was purchased from MTI Corporation. From the material datasheet, the reported thickness and porosity of the PP-PE-PP separator were 25 μm and 0.39, respectively. A polytetrafluoroethylene (PTFE) separator was

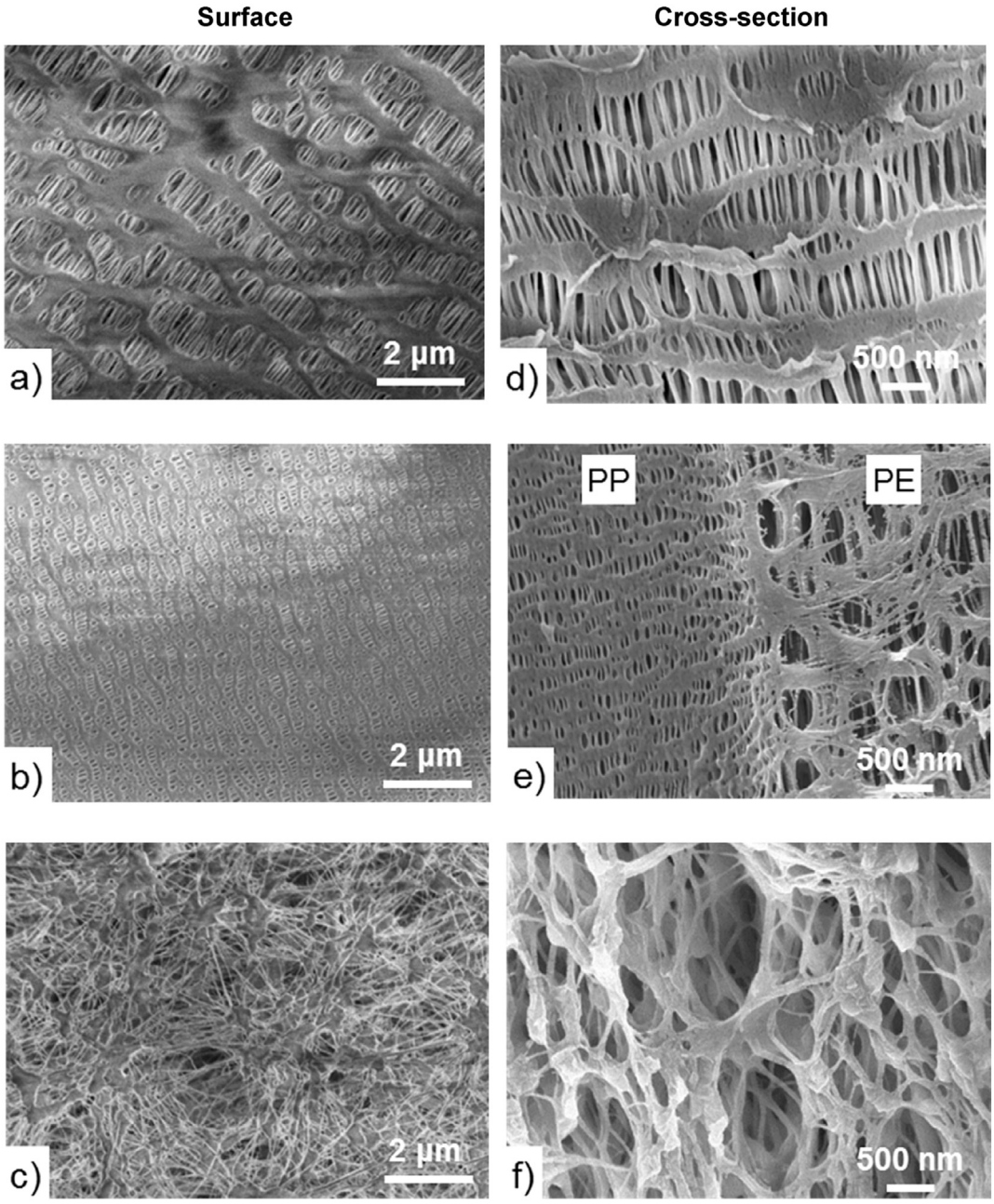

Fig. 2. Electron microscopy images of the separators. Surface morphology determined by SEM a) Celgard 2500, b) PP-PE-PP, c) PTFE. Cross-sectional morphology determined by SEM d) Celgard 2500, e) PP-PE-PP, f) PTFE.

provided by the 3M Company without a material datasheet.

Inside the glove box, the thickness (l) of each separator was measured at several locations using a micrometer (Mitutoyo). On average, the thicknesses of the Celgard 2500, PP-PE-PP, and PTFE separators were determined to be 25.4 ± 0.6 μm, 25.5 ± 0.5 μm, and 36.6 ± 0.8 μm, respectively. The uncertainty of all quantities reported in this paper corresponds to the standard deviation of several measurements. These results are listed in Table 1.

The separator porosity (ε) is defined as the ratio of the pore volume (V_{pore}) within the separator to the volume of the dry separator including the pores ($V_{separator,dry}$).

$$\varepsilon = \frac{V_{pore}}{V_{separator,\ dry}} \tag{1}$$

Experimentally, ε was determined from the following equation [4].

$$\varepsilon = 1 - \frac{M_{separator,\ dry}}{V_{separator,\ dry} \cdot \rho_P} \tag{2}$$

where $M_{separator,dry}$ is the experimentally determined weights of the dry separator disks. ρ_P is the density of the neat polymer used to make the separator, i.e. 0.9 g cm^3 for PP and PE and 2.2 g cm^3 for PTFE [16]. The average experimentally determined porosity of the Celgard 2500, PP-PE-PP, and PTFE separators were 0.53 ± 0.03, 0.39 ± 0.03, and 0.71 ± 0.03, respectively. The experimental thicknesses and porosities of the Celgard 2500 and PP-PE-PP separators are similar to those reported on the manufacturer material

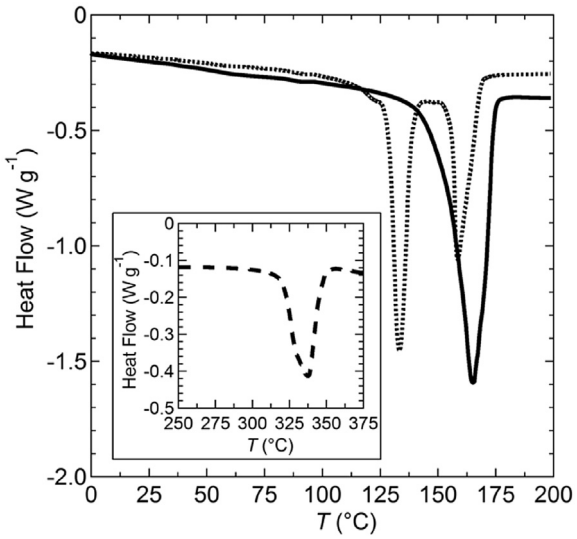

Fig. 3. DSC thermograms, heat flow as a function of the temperature, for the (solid line) Celgard 2500 and (dotted line) PP-PE-PP separator. The inset shows the thermogram of the (dashed line) PTFE separator. The heat flow is shown with exothermic peaks up.

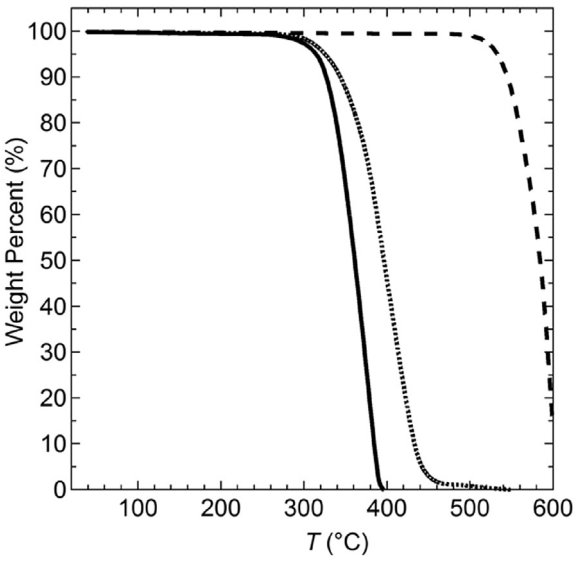

Fig. 4. Thermogravimetric curves, weight percent as a function of the temperature, for the (solid line) Celgard 2500, (dotted line) PP-PE-PP, and (dashed line) PTFE separators.

datasheet. Note that calculations requiring l and ε in this paper are based on the experimentally determined values given in Table 1.

The electrolyte uptake (EU) was measured for the three electrolytes in each of the three separators. The electrolyte uptake is defined as:

$$EU = \frac{M_{\text{separator, wet}} - M_{\text{separator, dry}}}{M_{\text{separator, dry}}} \quad (3)$$

where $M_{\text{separator,wet}}$ is the separator mass after soaking in the electrolyte for an hour in which the excess of electrolyte on the separator surface was removed with a filter paper. The average EU values for each electrolyte-separator composite combination are listed in Table 2. These values are based on five independent measurements and the error bars represent the standard deviation.

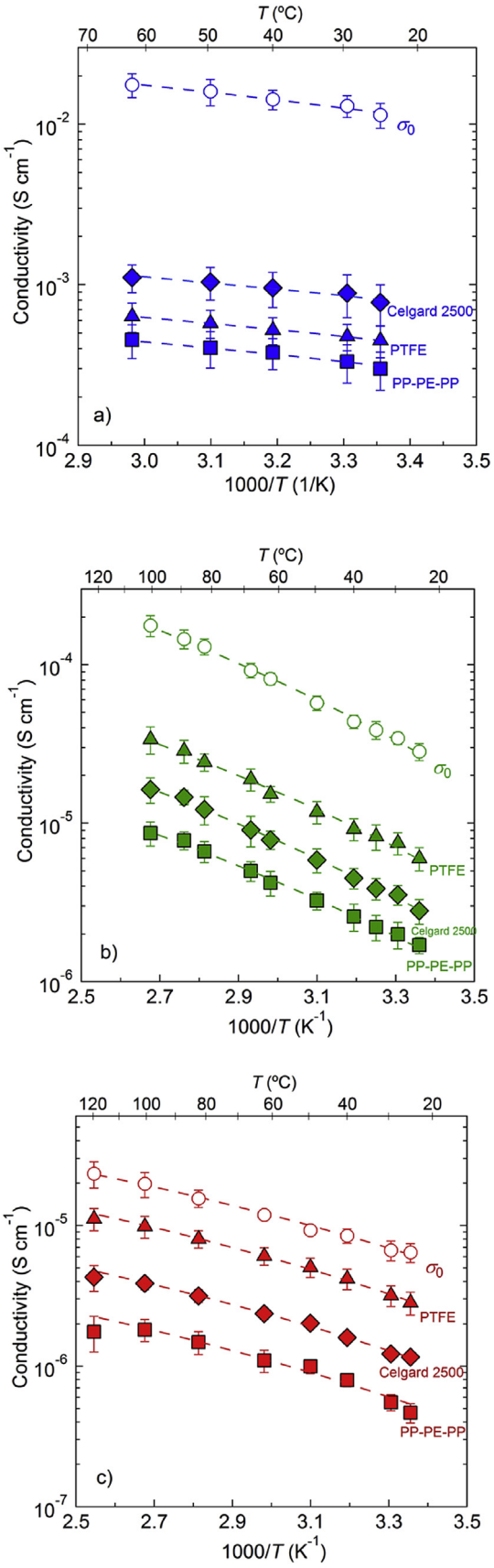

Fig. 5. Conductivity of neat electrolytes (σ_0) and electrolyte-separator composites (σ) as a function of 1000/T. a) $LiPF_6$/(EC-DMC), b) $PFPE_{E10H}$, and c) $PFPE_{DMC}$. The open symbols correspond to σ_0. The filled symbols correspond to σ, (◆) Celgard 2500, (■) PP-PE-PP, and (▲) PTFE separators. The dashed lines correspond to the VTF fits, and the fit parameters are listed in Table 3.

Table 3
VTF parameters obtained by fitting conductivity data. The T_0 values were chosen to be $T_g - 50$, with T_g values of 201.7 K and 183.2 K for the $LiPF_6$/(EC-DMC) [26] and the two PFPE-based electrolytes [13], respectively.

	$LiPF_6$/(EC-DMC)		$PFPE_{E10H}$		$PFPE_{DMC}$	
	A (S $K^{0.5}$ cm^{-1})	B (kJ mol^{-1})	A (S $K^{0.5}$ cm^{-1})	B (kJ mol^{-1})	A (S $K^{0.5}$ cm^{-1})	B (kJ mol^{-1})
Neat electrolyte	2.11	2.85	2.31×10^{-1}	8.46	5.78×10^{-3}	5.47
Celgard 2500	0.10	2.38	1.86×10^{-2}	8.13	1.43×10^{-3}	5.87
PP-PE-PP	0.04	2.49	8.42×10^{-3}	7.80	6.93×10^{-3}	5.92
PTFE	0.06	2.41	3.34×10^{-2}	7.92	3.73×10^{-3}	5.91

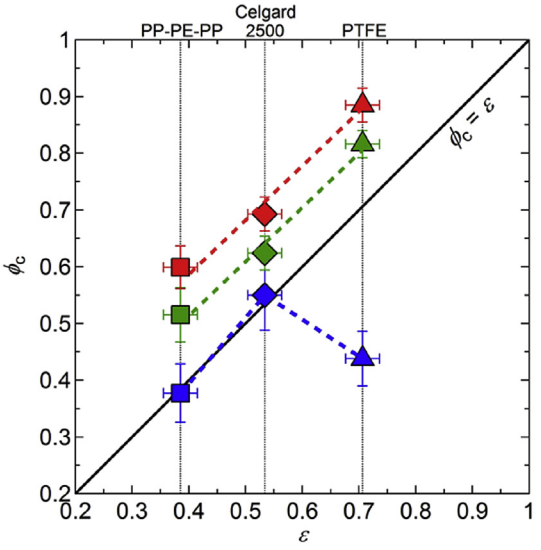

Fig. 6. Volume fraction of electrolyte (φ_c) as a function of the separator porosity (ε), (◆) Celgard 2500, (■) PP-PE-PP, and (▲) PTFE separators, while (blue) $LiPF_6$/(EC-DMC), (green) $PFPE_{E10H}$, and (red) $PFPE_{DMC}$ electrolytes. The dashed lines are guides to the eyes. The straight line represents $\varphi_c = \varepsilon$. (For interpretation of the references to colour in this figure legend, the reader is referred to the web version of this article.)

2.3. Separator characterizations

Scanning electron microscopy (SEM) experiments on cross sections of the separators were performed at the Molecular Foundry at the Lawrence Berkeley National Laboratory. A piece of the porous separator was cryo-fractured in liquid nitrogen and the sample was sputter-coated with 2 nm of gold prior to the SEM experiment. SEM was done on a Zeiss Gemini Supra 55 VP-SEM instrument with an acceleration voltage of 5 keV. These electron micrographs provide the cross-sectional morphology of the separators in dry state. In addition, SEM was also used to image the surface of the separators in dry state with an acceleration voltage of 5–15 keV.

The thermal properties of the separators were studied via differential scanning calorimetry (DSC) experiments. Inside the glove box, dry separator samples were sealed in aluminum hermetic pans and DSC experiments were performed on a TA Instruments DSC Q200 instrument. The samples were first held at −10 °C before being heated at 10 °C min^{-1} up to 200 °C for the Celgard 2500 and PP-PE-PP separators, and up to 400 °C for the PTFE separator. The onset melting temperatures (T_m) of the PE, PP, or PTFE polymers were determined from the endothermic peaks.

Thermogravimetric analysis (TGA) was carried out to determine the thermal stability of each separator. The samples were placed in an aluminum pan and heated up to 500 °C at 10 °C min^{-1} under a constant flow of argon gas to determine the onset temperature of the separator degradation (T_d) corresponding to a 5% mass loss.

2.4. Symmetric cell assembly and testing

Standard 2325 coin cells were used to determine the conductivity of electrolyte-separator composite (σ). These cells contained two stainless steel disks of area S which served as electrodes. Inside the Argon glove box, the electrolyte-separator composite was placed between the electrodes. The coin cells were sealed in a custom-built hydraulic crimping machine at 200 PSI manufactured by the National Research Council of Canada. A similar external sealing pressure was applied to each coin cell leading to identical compression of the cell assembly. After assembly, the coin cells were placed in a custom-made heating box located inside the argon glove box and connected to a multipotentiostat (VMP3, Bio-Logic SAS). Impedance spectroscopy measurements were made using an ac voltage between 10 and 40 mV in a frequency range between 10^6 and 1 Hz. Samples were heated from room temperature up to 120 °C in 10 or 20 °C steps, cooled in the same steps and re-heated to 120 °C in the same steps. For the conventional liquid electrolyte, $LiPF_6$/(EC-DMC), the maximum temperature set was 60 °C. A typical impedance spectrum of the $PFPE_{E10H}$-Celgard 2500 composite at 40 °C is shown in Fig. 1. For each temperature (T), the electrolyte resistance (R_{el}) was monitored as a function of time and the impedance spectra was recorded only when R_{el} became stable, typically after a 3 h waiting period. The equilibrated value of R_{el} was extracted from the impedance spectra by fitting the data with an equivalent electrical circuit [17–19]. This circuit, shown in the inset of Fig. 1, is composed of the apparatus resistance (R_c) and inductance (L_c), in series with R_{el} in parallel with the electrolyte pseudo-capacitance (CPE_{el}), in series with the blocking electrode-electrolyte interface pseudo-capacitance (CPE_{int}). At each T considered, the conductivity of the electrolyte-separator composite is calculated by:

$$\sigma(T) = \frac{l}{S \cdot R_{el}(T)} \tag{4}$$

The average conductivity for each electrolyte-separator composite combination was determined from five independent measurements and the error bars represent the standard deviation. In addition, custom made stainless steel symmetric liquid cells were used to characterize the conductivity of the neat electrolytes (σ_0) [20]. The impedance spectra of the liquid cells are qualitatively similar to those of the coin cells. Our approach for determining σ_0 is given in Ref. [20].

3. Results and discussion

Surface morphologies of the separators, determined by SEM, are shown in Fig. 2a through c, while cross-sectional morphologies, determined by SEM, are shown in Fig. 2d through f. The surface of the Celgard 2500, shown in Fig. 2a, has elliptical pores uniformly

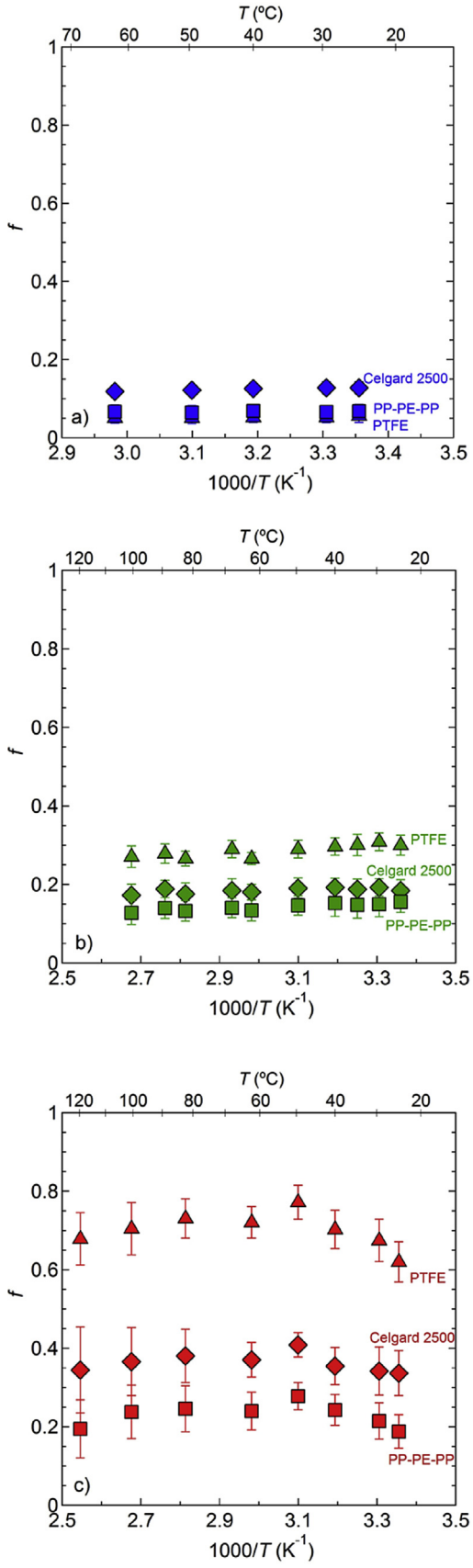

Fig. 7. Separator morphological factor f as a function of 1000/T. a) $LiPF_6$/(EC-DMC), b) $PFPE_{E10H}$, and c) $PFPE_{DMC}$ electrolytes. The filled symbols correspond to (◆) Celgard 2500, (■) PP-PE-PP, and (▲) PTFE separators.

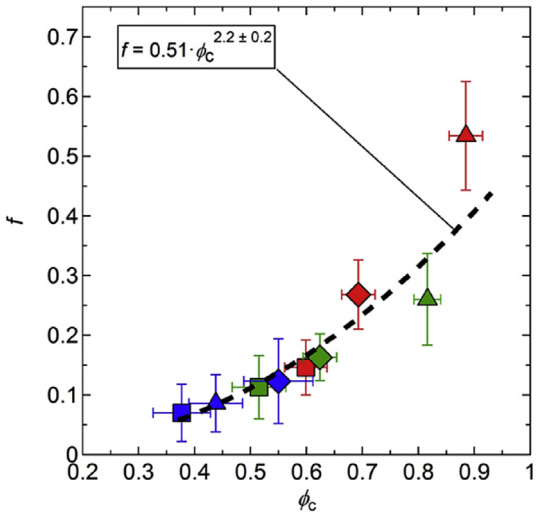

Fig. 8. Separator morphological factor (f) as a function the volume fraction of electrolyte (φ_c) at 30 °C, (◆) Celgard 2500, (■) PP-PE-PP, and (▲) PTFE separators, while (blue) $LiPF_6$/(EC-DMC), (green) $PFPE_{E10H}$, and (red) $PFPE_{DMC}$ electrolytes. (For interpretation of the references to colour in this figure legend, the reader is referred to the web version of this article.)

distributed in a PP matrix. The major axes of the ellipses are more or less aligned [3,21]. From Fig. 2a, the averaged major and minor diameters are 0.39 ± 0.15 μm and 0.059 ± 0.019 μm, respectively. These values are in agreement with those reported by Sarada et al. [21] Our experimental data are also consistent with the average pore size of 0.209 μm in length by 0.054 μm in width given by the manufacturer [2]. Elliptical pores are also observed in the cross-section of Celgard 2500, as seen in the SEM Fig. 2d. The averaged major and minor diameters in the cross-sectional view are 0.37 ± 0.18 μm and 0.056 ± 0.02 μm, respectively. The surface of the PP-PE-PP separator imaged by SEM in Fig. 2b also shows elliptical pores with averaged major and minor diameter of 0.12 ± 0.05 μm and 0.061 ± 0.017 μm, respectively. The cross-section of this separator reveals an inner PE layer, on the right side in Fig. 2e, that is significantly more porous than the PP layer. The PP-PE-PP separator appears to have a morphology very similar to that of the commercial trilayer Celgard 2325 separator [3]. In Fig. 2c and f, we show the surface and cross-section of the PTFE separator. The separator shows a complex porous network with a large porosity. This microstructure is characteristic of non-woven separators [2]. In average pore size is 0.35 ± 0.14 μm.

Fig. 3 shows the DSC thermograms of the Celgard 2500 and PP-PE-PP separators, while the PTFE thermogram is shown in the inset. For the Celgard 2500 separator, T_m is 154 °C, corresponding to the melting of PP [2]. For the multilayer PP-PE-PP separator, two melting temperatures are observed at 129 °C and 156 °C, corresponding to the melting of the PE and PP phase, respectively [3,6]. The PTFE separator exhibits a melting peak at a higher temperature, 321 °C, in agreement with the value reported by Laman et al. [22] The degradation temperatures, T_d determined by TGA, shown in Fig. 4, were 311 °C for Celgard 2500, 347 °C for PP-PE-PP, and 527 °C for PTFE. The values of T_m and T_d are given in Table 1.

The conductivity of electrolyte-separator composites containing $LiPF_6$/(EC-DMC) and that of the neat electrolyte, σ and σ_0, respectively, are plotted as a function of the inverse of the temperature in Fig. 5a. The conductivity of the neat electrolyte increases from 1.14×10^{-2} S cm^{-1} at 24.9 °C to 1.76×10^{-2} S cm^{-1} at 60 °C. These values are in good agreement with those reported in literature [23–26]. The conductivities of the electrolyte-separator composites

are about one order of magnitude lower than those of the neat electrolyte. The room temperature value of the ratio of σ_0 to σ, usually defined as the MacMullin number [5,27], is consistent with literature data [12]. The highest conductivity is obtained in the Celgard 2500-containing composite, and the lowest was obtained in the PP-PE-PP-containing composite. Fig. 5b and c shows σ and σ_0 as a function of the inverse of the temperature of the $PFPE_{E10H}$ and $PFPE_{DMC}$ electrolyte-separator composites. The conductivity of neat $PFPE_{E10H}$- and $PFPE_{DMC}$-based electrolytes are two to three orders of magnitude lower than σ_0 of $LiPF_6$/(EC-DMC). Interestingly, for the two PFPE electrolytes, the highest conductivity in coin cells is obtained when the PTFE separator is used.

The conductivity of all our samples is consistent with the Vogel–Tamman–Fulcher (VTF) equation [28–30]:

$$\sigma(T) = \frac{A}{\sqrt{T}} \cdot \exp\left(\frac{-B}{R \cdot (T - T_0)}\right) \tag{5}$$

where R is the gas constant and T_0 is the glass transition temperature (T_g) minus 50 K [31]. Based on literature data, $T_g = 201.7$ K for $LiPF_6$/(EC-DMC) [26] and 183.2 K for the two PFPE electrolytes [13]. The dashed lines in Fig. 5a through c represent least-squared fits of the data. The parameters A and B, thus obtained, are given in Table 3.

The electrolyte uptake data given in Table 2 is used to estimate the volume fraction of electrolyte in the separator, φ_c.

$$\varphi_c = \frac{1}{1 + \frac{1}{EU} \cdot \frac{\rho_{el}}{\rho_p}} \tag{6}$$

In Fig. 6 we plot φ_c as a function of ε. The line in Fig. 6 represents $\varphi_c = \varepsilon$. If the electrolyte were to occupy the pores in the separator fully without distorting the separator, then the data would lie on this line. This is observed for the $LiPF_6$/(EC-DMC)-Celgard 2500 and $LiPF_6$/(EC-DMC)-PP-PE-PP composites. The $LiPF_6$/(EC-DMC)-PTFE composite exhibits a φ_c value lower than ε. We attribute this to incomplete filling of the pores due to wettability problems. Surprisingly, the PFPE based electrolytes exhibit φ_c values greater than ε. This implies that PFPE electrolytes distort the separators due to swelling.

We assumed that the conductivity of the electrolyte-separator composites is given by:

$$\sigma = f \cdot \sigma_0 \cdot \varphi_c \tag{7}$$

where f is a morphological factor that accounts for the tortuosity and connectivity of the pores [32]. A similar equation is often used to describe the conductivity of block copolymer electrolytes [33–35]. The value of f reflects the efficacy of the separator. For an ideal separator with no tortuosity and a perfectly connected pore structure, f would be unity. Since σ, σ_0, and φ_c have been measured (Fig. 5, Table 2) we can compute f for each of the electrolyte-separator composites. The temperature dependence of f thus obtained is given in Fig. 7. As expected, f of a given composite is independent of the temperature. It is interesting to note that the value of f for $PFPE_{DMC}$-PTFE composite is as high as 0.7, a value significantly higher than that of all of the composites containing the $LiPF_6$/(EC-DMC) electrolyte, which lie between 0.05 and 0.13.

In Fig. 8, we plot f versus φ_c. In spite of differences in the conductivity of the neat electrolyte, porosity, and electrolyte uptake, data from all of the systems collapse onto a master curve. The dashed curve in Fig. 8 is a power law fit that yields $f = 0.51 \cdot \varphi_c^{2.2\pm0.2}$. In other words, the conductivity of our electrolyte-separator composites is proportional to $\varphi_c^{3.2\pm0.2}$. Our data are consistent with the Bruggeman relationship [7]. The data in Fig. 8 correspond to 30 °C (near room temperature). Note however that f is essentially independent of temperature (Fig. 7).

Most of the literature on the conductivity of electrolyte-separator composites is based on the following equation: [5,7,12,36]

$$\sigma = \frac{\sigma_0 \cdot \varepsilon}{\tau} = f \cdot \sigma_0 \cdot \varepsilon \tag{8}$$

where it is assumed that the electrolyte fills the pores, i.e. $\varphi_c = \varepsilon$, and τ, the tortuosity, is equal to $1/f$. Examining Figs. 6 and 8, it should be clear that our conductivity data from both carbonate- and PFPE-based electrolytes are inconsistent with equation (8). A master curve is only obtained when electrolyte uptake is taken into account. However, conductivity data from the carbonate-based electrolyte in polyolefin separators are consistent with equation (8). In a related study, Quartarone et al. showed that the conductivity of a carbonate-based electrolyte in polyvinylidene fluoride gel well above the percolation threshold was proportional to $EU^{3.24\pm0.3}$ [37]. The power law exponent obtained by Quartarone et al. is within experimental error of that reported in Fig. 8. We note that EU and φ_c are proportional to each other in the large electrolyte uptake limit (see equation (6)).

4. Conclusion

We report on the morphology and thermal properties of three porous separators: a single layer Celgard 2500 separator, a trilayer PP-PE-PP separator, and a PTFE separator. The pore morphologies within the separators are widely different. In spite of this, we demonstrate that the conductivity (σ) of carbonate- and perfluoropolyether-based electrolyte-separator composites depends mainly on the electrolyte uptake, and follows a master equation, $\sigma = 0.51 \cdot \sigma_0 \cdot \varphi_c^{3.2\pm0.2}$, where φ_c is the volume fraction of electrolyte in the separator. The conductivity of the neat electrolytes used in this study, σ_0, varied from 6.46×10^{-6} to 1.76×10^{-2} S cm^{-1}. The master equation applies to electrolytes that completely filled the pores in the separator, electrolytes that swell the separator, as well as electrolytes that only partially wet the separator pores.

Acknowledgements

This work was supported as part of the Center for Mesoscale Transport Properties, an Energy Frontier Research Center supported by the U.S. Department of Energy, Office of Science, Basic Energy Sciences, under award #DE-SC0012673.

Abbreviations

PFPE	perfluoropolyether
PE	polyethylene
PP	polypropylene
PTFE	polytetrafluoroethylene
LiTFSI	lithium bis(trifluoromethanesulfonyl)imide
$LiPF_6$	lithium hexafluorophosphate
DMC	dimethyl carbonate
EC	ethylene carbonate
A	Vogel-Tammann-Fulcher prefactor [S K$^{0.5}$ cm^{-1}]
B	Vogel-Tamman-Fulcher activation energy [kJ mol^{-1}]
EU	electrolyte uptake
f	separator morphological factor
l	separator thickness [μm]
$M_{separator,dry}$	dry separator mass [g]

$M_{separator,wet}$ separator mass after soaking in the electrolyte for an hour [g]
R gas constant [J K^{-1} mol^{-1}]
R_{el} electrolyte resistance [Ω]
S stainless-steel disk area [cm^2]
T temperature [K or °C]
T_g glass transition temperature [K]
T_0 T_g minus 50 K
T_m onset of melting temperature [°C]
T_d onset temperature of the separator degradation [°C]
V_{pore} pore volume in the separator [cm^3]
$V_{separator,dry}$ volume of dry separator disk [cm^3]
ε separator porosity
ρ_{el} density of the electrolyte
ρ_P density of the neat polymer used to make the separator [g cm^3]
σ conductivity of the electrolyte-separator composite [S cm^{-1}]
σ_o neat conductivity [S cm^{-1}]
τ separator tortuosity
φ_c volume fraction of the electrolyte in the separator

References

[1] M. Winter, R.J. Brodd, Chem. Rev. 104 (2004) 4245–4269.
[2] S.S. Zhang, J. Power Sources 164 (2007) 351–364.
[3] P. Arora, Z.J. Zhang, Chem. Rev. 104 (2004) 4419–4462.
[4] H. Lee, M. Yanilmaz, O. Toprakci, K. Fu, X. Zhang, Energy Environ. Sci. 7 (2014) 3857–3886.
[5] K.M. Abraham, Electrochim. Acta 38 (1993) 1233–1248.
[6] G. Venugopal, J. Moore, J. Howard, S. Pendalwar, J. Power Sources 77 (1999) 34–41.
[7] K.K. Patel, J.M. Paulsen, J. Desilvestro, J. Power Sources 122 (2003) 144–152.
[8] I.V. Thorat, D.E. Stephenson, N.A. Zacharias, K. Zaghib, J.N. Harb, D.R. Wheeler, J. Power Sources 188 (2009) 592–600.
[9] Y. Saito, W. Morimura, R. Kuratani, S. Nishikawa, J. Phys. Chem. C 119 (2015) 4702–4708.
[10] J.Y. Song, Y.Y. Wang, C.C. Wan, J. Electrochem. Soc. 147 (2000) 3219–3225.
[11] A. Chagnes, B. Carré, P. Willmann, R. Dedryvère, D. Gonbeau, D. Lemordant, J. Electrochem. Soc. 150 (2003) A1255–A1261.
[12] D. Djian, F. Alloin, S. Martinet, H. Lignier, J.Y. Sanchez, J. Power Sources 172 (2007) 416–421.
[13] D.H.C. Wong, J.L. Thelen, Y. Fu, D. Devaux, A.A. Pandya, V.S. Battaglia, N.P. Balsara, J.M. DeSimone, Proc. Natl. Acad. Sci. U.S.A. 111 (2014) 3327–3331.
[14] D.H.C. Wong, A. Vitale, D. Devaux, A. Taylor, A.A. Pandya, D.T. Hallinan, J.L. Thelen, S.J. Mecham, S.F. Lux, A.M. Lapides, P.R. Resnick, T.J. Meyer, R.M. Kostecki, N.P. Balsara, J.M. DeSimone, Chem. Mater. 27 (2015) 597–603.
[15] A.E. Ozcam, N. Petzetakis, S. Silverman, A.K. Jha, N.P. Balsara, Macromolecules 46 (2013) 9652–9658.
[16] J. Brandrup, E.H. Immergut, Polymer Handbook, third ed., John Wiley & Sons, New York, 1989.
[17] J. Ross Macdonald, J. Electrochem. Soc. 135 (1988) 2274–2279.
[18] R. Bouchet, S. Lascaud, M. Rosso, J. Electrochem. Soc. 150 (2003) A1385–A1389.
[19] D. Devaux, R. Bouchet, D. Glé, R. Denoyel, Solid State Ion. 227 (2012) 119–127.
[20] A.A. Teran, M.H. Tang, S.A. Mullin, N.P. Balsara, Solid State Ion. 203 (2011) 18–21.
[21] T. Sarada, L.C. Sawyer, M.I. Ostler, J. Membr. Sci. 15 (1983) 97–113.
[22] F.C. Laman, M.A. Gee, J. Denovan, J. Electrochem. Soc. 140 (1993) L51–L53.
[23] E.J. Plichta, W.K. Behl, J. Power Sources 88 (2000) 192–196.
[24] M. Dahbi, F. Ghamouss, F. Tran-Van, D. Lemordant, M. Anouti, J. Power Sources 196 (2011) 9743–9750.
[25] L. Niedzicki, S. Grugeon, S. Laruelle, P. Judeinstein, M. Bukowska, J. Prejzner, P. Szczeciński, W. Wieczorek, M. Armand, J. Power Sources 196 (2011) 8696–8700.
[26] P.E. Stallworth, J.J. Fontanella, M.C. Wintersgill, C.D. Scheidler, J.J. Immel, S.G. Greenbaum, A.S. Gozdz, J. Power Sources 81–82 (1999) 739–747.
[27] R.B. MacMullin, G.A. Muccini, AIChE J. 2 (1956) 393–403.
[28] H. Vogel, Phys. Z. 22 (1921) 645–646.
[29] V.G. Tamman, W. Hesse, Z. Anorg. Allg. Chem. 156 (1926) 245–257.
[30] G.S. Fulcher, J. Am. Ceram. Soc. 8 (1925) 339–355.
[31] J.L. Souquet, M. Duclot, M. Levy, Solid State Ion. 85 (1996) 149–157.
[32] D.T. Hallinan, N.P. Balsara, Annu. Rev. Mater. Res. 43 (2013) 503–525.
[33] A. Panday, S. Mullin, E.D. Gomez, N. Wanakule, V.L. Chen, A. Hexemer, J. Pople, N.P. Balsara, Macromolecules 42 (2009) 4632–4637.
[34] I. Villaluenga, X.C. Chen, D. Devaux, D.T. Hallinan, N.P. Balsara, Macromolecules 48 (2015) 358–364.
[35] W.-S. Young, W.-F. Kuan, T.H. Epps, J. Polym. Sci. B Polym. Phys. 52 (2014) 1–16.
[36] F.L. Tye, J. Power Sources 9 (1983) 89–100.
[37] E. Quartarone, P. Mustarelli, A. Magistris, J. Phys. Chem. B 106 (2002) 10828–10833.